

# Impact of microgravity on retinal neuroimmune responses and visual dysfunction in rats

Jin-Shuo Liu<sup>1</sup>, Nai-Qin Yan<sup>2</sup>, Ying-Yan Mao<sup>3,4</sup>, Chen Xin<sup>3,4</sup>, Da-Peng Mou<sup>3</sup>, Xin-Xiao Gao<sup>1</sup>, Jia Guo<sup>1</sup>, Ning-Li Wang<sup>3,4</sup>, Si-Quan Zhu<sup>1</sup>

<sup>1</sup>Department of Ophthalmology, AnZhen Hospital, Capital Medical University, Beijing 100011, China

<sup>2</sup>Department of Rehabilitation, Daqing Rehabilitation Hospital, Daqing 163453, Heilongjiang Province, China

<sup>3</sup>Beijing Institute of Ophthalmology, Beijing Tongren Hospital, Capital Medical University, Beijing 100005, China

<sup>4</sup>Beijing Ophthalmology and Visual Sciences Key Laboratory, Beijing Tongren Eye Center, Beijing Tongren Hospital, Capital Medical University, Beijing 100054, China

**Correspondence to:** Si-Quan Zhu. Department of Ophthalmology, AnZhen Hospital, Capital Medical University, Beijing 100011, China. siquanzhu@qq.com

Received: 2025-02-10 Accepted: 2025-05-15

## Abstract

• **AIM:** To analyze visual dysfunction in rats under simulated weightlessness (SW) by examining trans-laminar cribriform pressure difference (TLCPD) and neuroimmune responses.

• **METHODS:** The 72 male Sprague-Dawley rats were randomly assigned into two groups (ground control and hindlimb unloading-simulated microgravity) using stratified randomization, with each group further subdivided into three exposure durations: SW 2-week (SW-2W), 4-week (SW-4W), and 8-week (SW-8W),  $n=12$  per subgroup. At the designated time points for each group, intraocular pressure (IOP) and intracranial pressure (ICP) were measured, and the trans-laminar cribriform pressure difference (TLCPD) was calculated. Additionally, optomotor response (OMR), electroretinography (ERG), and optical coherence tomography (OCT) were performed. The number of retinal ganglion cells (RGCs) was quantified via immunofluorescence, the activation of astrocytes and microglial cells was determined, and Sholl analysis was conducted to assess the function and morphology of microglial cells. Data were analyzed with SPSS and GraphPad Prism ( $P<0.05$ ).

• **RESULTS:** Under prolonged simulated microgravity, rats exhibited a progressive increase in both IOP and ICP, with the most pronounced rise observed at 8wk. Concurrently,

the TLCPD shifted from a negative value in controls to a positive value. These pressure alterations were associated with retinal dysfunction, as evidenced by significant reductions in ERG b-wave and photopic negative response (PhNR) amplitudes. OCT and histological analyses revealed subtle photoreceptor layer damage: while the inner nuclear layer (INL) thickness remained relatively unchanged, the outer nuclear layer (ONL) thinned significantly, and the nerve fiber layer-ganglion cell layer complex thickness (NFL-GCL) complex initially thickened before later thinning. Immunofluorescence further demonstrated marked neuroimmune activation, with astrocytes transitioning from having large cell bodies with small, elongated, sparse processes to a phenotype characterized by compact, enlarged nuclei and aggregated processes, alongside notable RGC loss.

• **CONCLUSION:** Based on the results from the simulated microgravity rat model, microgravity-induced changes in dual-chamber pressure, and neuroimmune responses in the retina may play a key role in visual dysfunction. Specifically, the activation of retinal neuroimmune cells (astrocytes and microglial cells) induced by mechanical stress appears to be central to retinal and optic nerve damage.

• **KEYWORDS:** simulated weightlessness; microgravity; neuroimmune; microglia; astrocyte activation

**DOI:10.18240/ijo.2025.08.01**

**Citation:** Liu JS, Yan NQ, Mao YY, Xin C, Mou DP, Gao XX, Guo J, Wang NL, Zhu SQ. Impact of microgravity on retinal neuroimmune responses and visual dysfunction in rats. *Int J Ophthalmol* 2025;18(8):1409-1425

## INTRODUCTION

Long-duration spaceflight presents numerous challenges to astronauts' health, with alterations in the visual system being among the most prominent. Studies have shown that around 70% of astronauts who participate in missions lasting six months or more experience ocular abnormalities, a condition collectively referred to as spaceflight-associated neuro-ocular syndrome (SANS)<sup>[1]</sup>. Rather than being a singular

disease, SANS encompasses a range of symptoms, including choroidal folds and swelling, optic disc edema (papilledema), globe flattening, optic nerve sheath distension, retinal nerve fiber layer thickening, hyperopic shifts, and cotton wool spots<sup>[2-3]</sup>. While the prevalence of these symptoms varies, retinal thickening is commonly observed in the majority of astronauts. As the length of space missions continues to increase, research into SANS has become increasingly important<sup>[4-5]</sup>.

Numerous theoretical hypotheses have been proposed regarding the pathogenesis of SANS. A frequently discussed hypothesis involves the imbalance between intracranial pressure (ICP) and intraocular pressure (IOP), which is thought to result from cephalad fluid shifts. These mismatch may lead to an increased translaminar pressure gradient, thereby potentially damaging the optic nerve<sup>[1,6-7]</sup>. In addition, genetic, metabolic, and environmental factors are believed to play a role, possibly triggering vascular endothelial dysfunction and the formation of edema<sup>[8]</sup>. Other contributing factors include ischemia, oxidative stress, cosmic radiation exposure, elevated carbon dioxide levels, and dietary and exercise changes<sup>[6,9-10]</sup>. To gain a deeper understanding of SANS pathogenesis, ground-based simulation experiments have become essential. Rodents subjected to tail suspension and/or hindlimb unloading are used to replicate microgravity conditions comparable to human head-down tilt<sup>[11-12]</sup>. These models have shown vascular alterations that align with findings from spaceflight studies<sup>[13]</sup>. Moreover, electroretinography (ERG) and optical coherence tomography (OCT) have emerged as valuable techniques for assessing retinal functional and structural changes, offering indispensable tools for studying the effects of microgravity on the retina<sup>[14-15]</sup>. Rodríguez-Arzate *et al*<sup>[14]</sup> highlighted the potential of non-invasive ERG to monitor retinal electrophysiological activity, which proves beneficial in early diagnosis and treatment, particularly for retinal degeneration, diabetes, and neurodegenerative diseases. Similarly, Takita *et al*<sup>[15]</sup> emphasized that ERG and visual evoked potential (VEP) systems are effective in evaluating retinal function, revealing localized changes in retinal activity linked to retinal damage, and aligning closely with histological findings<sup>[16]</sup>. Notably, studies have shown that, under prolonged simulated microgravity, albino rats demonstrate more pronounced ocular structural and functional alterations compared to pigmented rats, particularly in ERG, VEP, and fundus vascular changes. These differences may be related to alterations in melanin synthesis-related proteins in retinal pigment epithelial cells<sup>[17]</sup>. Retinal ganglion cells (RGCs) are the essential output neurons of the mammalian retina, with their axons forming the primary components of the optic nerve. The optic nerve exits the eye posteriorly and travels to the brain, where RGC

axons synapse with higher-order neurons. Along this pathway, two main forces affect RGC axons: IOP at the anterior optic nerve head and ICP at the posterior optic nerve head and along the optic nerve itself<sup>[18-19]</sup>. Increases in either ICP or IOP, whether idiopathic or secondary, can lead to vision-threatening conditions such as SANS, idiopathic intracranial hypertension (IIH; ICP), and glaucoma IOP<sup>[20-21]</sup>. Under microgravity conditions, the redistribution of fluids towards the head induces a series of complex pathological changes, including cranial venous congestion, choroidal blood flow stasis, and retinal thickening. Prolonged exposure to elevated ICP and cerebrospinal fluid (CSF) stagnation may further lead to retinal ischemia and impaired perfusion<sup>[19]</sup>. Despite this, few studies have investigated the impact of trans-laminar cribrosa pressure difference (TLCPD) in the hindlimb suspension rat model, leaving it uncertain whether visual dysfunction associated with microgravity is linked to alterations in TLCPD. In prior work, our studies with the low intracranial pressure (LICP) rat model, which is characterized by reduced CSF pressure, revealed early astrocyte activation in the retina. These glial cells secrete cytokines or neurotrophic factors, potentially contributing to damage to the blood-retinal barrier (BRB) and retinal RGC injury<sup>[22]</sup>. Both microglial cells and astrocytes are pivotal for retinal development and functionality, particularly in retinal degenerative diseases, by supporting the health of retinal neurons and regulating retinal blood flow<sup>[23]</sup>. However, research on the activation and functional roles of neuroimmune cells in the retina under microgravity remains scarce. Whether excessive activation of immune cells leads to visual impairment is still uncertain, and at present, we lack conclusive evidence on this matter.

This study was designed to simulate the effects of prolonged microgravity through a tail suspension model, aiming to investigate its impact on visual function and retinal structural changes. Specifically, we assessed alterations in IOP, ICP, and computed the TLCPD. Retinal function was also evaluated, and immunofluorescence staining was employed to examine astrocytes and microglial cells within the retina. Furthermore, Sholl analysis was conducted to explore the morphology and functionality of microglial cells. By analyzing neuroimmune responses across different exposure durations, this research offers valuable insights into the potential ocular health risks associated with extended microgravity exposure.

## **MATERIALS AND METHODS**

**Ethical Approval** Protocols for this investigation received full ethical approval from the Institutional Animal Care and Use Committee at Capital Medical University (AEEI-2024-030), ensuring strict compliance with ARVO's Statement for the Use of Animals in Ophthalmic and Vision Research.

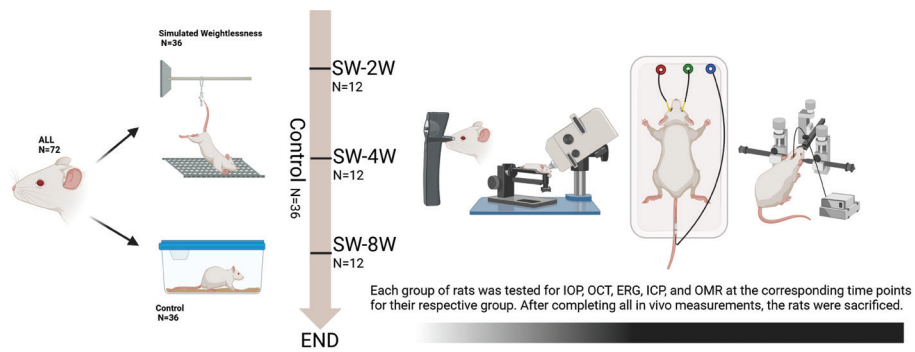


**Figure 1 Overall study timeline of SW in rats** The 72 male Sprague-Dawley rats were randomly assigned to two groups (ground control and hindlimb unloading-simulated microgravity) using stratified randomization, with each group further subdivided into three exposure durations: 2-week (SW-2W,  $n=12$ ), 4-week (SW-4W,  $n=12$ ), and 8-week (SW-8W,  $n=12$ ) subgroups. At the designated time points, each group underwent assessments, including IOP measurements, OCT, ERG, and OMR testing. At the final stage, ICP was measured through surgical procedures. Following the completion of all assessments, the rats were euthanized with a lethal dose of sodium pentobarbital. OMR: Optomotor response; ERG: Electroretinogram; ICP: Intracranial pressure; OCT: Optical coherence tomography; SW: Simulated weightlessness; IOP: Intraocular pressure.

The study utilized 72 male Sprague-Dawley rats (weight range: 250–300 g) sourced from Vital River Laboratory, Beijing, China. Through stratified randomization, animals were distributed into two primary groups: ground control ( $n=36$ ) and hindlimb unloading-induced microgravity simulation ( $n=36$ ). Both groups underwent temporal stratification into simulated weightlessness 2-week (SW-2W,  $n=12$ ), 4-week (SW-4W,  $n=12$ ), and 8-week (SW-8W,  $n=12$ ) observation periods. Figure 1 provides a schematic representation of the experimental design and group allocation strategy.

#### Establishment of the Simulated Weightlessness Model

The hindlimb unloading model, an established simulation of microgravity, was implemented according to validated protocols<sup>[24]</sup>. Following a 7-day acclimatization period, tail surfaces underwent preparatory treatment: initial cleansing followed by application of benzoin and rosin tinctures to optimize tape adhesion while preventing tissue injury. After complete drying, medical-grade adhesive tape (20 cm length) was secured to each tail, enabling suspension at a precise 30° head-down tilt within custom-fabricated enclosures. While forelimbs retained full mobility for access to food and water, hindlimb contact with cage flooring was systematically prevented. Environmental parameters were rigorously maintained (temperature: 23°C±1°C; relative humidity: 45%–55%; photoperiod: 12h light/12h dark cycles) throughout the experimental duration.

**IOP Measurement** IOP was assessed using a rebound tonometer (TonoLab, Icare, Helsinki, Finland) configured to the “rat” mode. Prior to measurements, rats were anesthetized with 3.5% isoflurane until the loss of the righting reflex, which typically occurred within 4–5min. IOP measurements were conducted daily between 9:00 and 11:00 *a.m.* The tonometer probe was carefully positioned perpendicular to the corneal

surface, and five consecutive readings were taken and averaged for each eye. To ensure accuracy, three such averages were obtained and recorded as the effective IOP for each eye.

**ICP Measurement** ICP monitoring commenced with isoflurane anesthesia (3% flow rate) administered through a precision gas delivery system. Anesthetic depth was verified by loss of righting reflex and absence of hindlimb withdrawal response to noxious stimuli. Following surgical site preparation (hair removal and disinfection), a midline scalp incision exposed the cranial vault through meticulous fascial and muscular dissection. Using stereotactic guidance, the Bregma landmark was identified, enabling precise burr hole placement (1.5 mm posterior, 0.8 mm lateral to Bregma) with controlled drilling to a 4 mm depth<sup>[20]</sup>. A 1 mm diameter dental drill (Dremel, Racine, WI, USA) facilitated gradual bone penetration. Upon dural breach confirmation, a 3 mm pressure transducer was advanced 1 mm into the cerebral parenchyma. The transducer interfaced with a biological signal acquisition system (PowerLab 16/35, AD Instruments, Australia) through a dedicated amplifier (Bridge Amp, AD Instruments, Australia), enabling continuous ICP monitoring at 1000 Hz sampling rate (mm Hg). Following signal stabilization, three consecutive measurement cycles provided mean ICP values. Post-procedural care included copious saline irrigation, layered closure (muscle, fascia), and skin approximation with aseptic precautions. Animals recovered on thermoregulated pads (about 20min) until complete anesthetic reversal.

**TLCPD Measurement** TLCPD was calculated as the difference between IOP and ICP for each time point. IOP and ICP values were obtained using standardized procedures. TLCPD was derived by subtracting the mean ICP value from the corresponding mean IOP value for each eye with results expressed in millimeters of mercury (mm Hg). Statistical

analyses were performed to evaluate changes in TLCPD across experimental groups and time points.

**Electroretinography** ERG was performed using the Espion Visual Electrophysiology System (Diagnosys, USA). Following  $\geq 6$ h of dark adaptation, pupil dilation was achieved through topical administration of compound tropicamide solution (Santen, Japan). Throughout the recording session, animals were maintained on thermoregulated pads to ensure physiological body temperature. Electrode placement involved a gold-ring corneal contact electrode (interface: carbomer gel; Bausch Lomb, Jinan, China) with subcutaneous reference and ground electrodes positioned in the cheek and tail regions, respectively. Dark-adapted flash stimuli ( $3.0 \text{ cd}\cdot\text{s}/\text{m}^2$ ) elicited characteristic waveforms, with specific analysis of a-wave, b-wave, and photopic negative response (PhNR) amplitudes. The PhNR component, observed subsequent to the b-wave, reflects primarily retinal RGCs activity with contributions from non-spiking amacrine cells<sup>[25]</sup>. Bilateral waveform amplitude measurements were systematically recorded for subsequent quantitative analysis.

**Optomotor Response** Visual Function Assessment Using Virtual Optomotor Tracking System (OptoMotry, Lethbridge, Canada). Rats were placed on a high platform located at the center of a testing chamber, which consisted of four computer monitors displaying rotating virtual spatial frequency gratings. A camera mounted on the ceiling of the chamber was used to monitor the rats' behavior. A psychophysiological staircase method was employed, where spatial frequency was randomly altered until the lowest threshold stimulus eliciting a visuomotor response at best contrast was identified. To independently assess visual function in each eye, clockwise or counterclockwise rotations were used. The mean spatial frequency threshold of each eye was recorded and analyzed.

**OCT** Retinal structural evaluation was performed using the Micron III OCT system (Phoenix Research Labs, Pleasanton, CA, USA). Under standardized anesthesia, pupil dilation was achieved with  $0.2 \text{ mg}/\text{mL}$  tropicamide phenylephrine, while corneal hydration was maintained using  $1.5\%$  hydroxyethylcellulose solution. Horizontal OCT scans centered on the optic nerve head were acquired through the integrated fundus camera, with scan orientation marked by a reference line. To enhance image quality, 30 consecutive scans were averaged, effectively reducing projection artifacts. Quantitative morphometric analysis employed Image J software (National Institutes of Health, Bethesda, MD, USA). At standardized positions ( $200 \mu\text{m}$  nasal and temporal to optic nerve head), layer-specific measurements included: total retinal thickness, nerve fiber layer-ganglion cell layer complex thickness (NFL-GCL) complex, and combined inner nuclear layer (INL) thickness, outer nuclear layer (ONL) thickness dimensions.

These parameters enabled systematic evaluation of retinal architecture.

**Pathological Examination of Retinal Sections** After the experiment, rats were deeply anesthetized *via* intraperitoneal injection of an overdose of pentobarbital sodium ( $50 \text{ mg}/\text{kg}$ ). *In situ* fixation of the eyeballs was performed by transcardial perfusion with saline followed by  $4\%$  paraformaldehyde ( $\text{pH } 7.4$ ). The enucleated eyes were post-fixed in fresh  $4\%$  paraformaldehyde for 24h at  $4^\circ\text{C}$ . Fixed samples were dehydrated through a graded ethanol series ( $50\%$ – $100\%$ ), cleared in xylene, and embedded in paraffin. Sagittal serial sections ( $4 \mu\text{m}$  thickness) were mounted on adhesive-coated slides. After deparaffinization in xylene and rehydration through graded ethanol, sections were stained with Harris hematoxylin (5min), differentiated in  $1\%$  acid alcohol (3–5s), blued in saturated lithium carbonate solution (1min), and counterstained with  $0.5\%$  eosin aqueous solution (1min). Sections were dehydrated in ethanol, cleared in xylene, and coverslipped with neutral resin. Retinal laminar structures were observed under a Leica light microscope at  $200\times$  magnification. Total retinal thickness and ONL thickness were measured using Image J software. For each sample, three non-consecutive sections were randomly selected, and five peri-optic disc fields per section were averaged for analysis. Key quality control parameters included fixation duration ( $24\pm 2$ h), section orientation (alignment of the cornea-optic nerve axis), and differentiation intensity (real-time microscopic monitoring of hematoxylin staining depth) to ensure clear tissue architecture and high-contrast staining.

**Immunofluorescence** The eyes of the rats were enucleated and fixed in  $4\%$  paraformaldehyde overnight at  $4^\circ\text{C}$ . For retinal flatmount preparation, the cornea, lens, and vitreous humor were carefully removed, and the isolated retina was immersed in  $0.5\%$  Triton X-100 for 4h. Subsequently, the retinas were blocked in  $1\%$  bovine serum albumin (BSA, A8010, Solarbio) for 2h, followed by overnight incubation with primary antibodies targeting RNA-binding protein with multiple splicing (RBPMS, 1:500, GTX118619, GeneTex), ionized calcium-binding adaptor molecule 1 (Iba-1, 1:500, Wako, Japan), and glial fibrillary acidic protein (GFAP, 1:500, #3670, CST, MA, USA). Iba-1 is a microglia-specific calcium-binding protein that indicates microglial activation. The following day, the retinas were incubated with fluorescent secondary antibodies for 1h in the dark at room temperature. Cell nuclei were counterstained with 4',6-diamidino-2-phenylindole (DAPI, ab104139, Abcam, Cambridge, USA). Non-overlapping images from the entire retina were captured using fluorescence microscopy (Leica, Wetzlar, Germany). Image J software (v1.53, National Institutes of Health, USA) was employed to quantify the number of RBPMS-stained

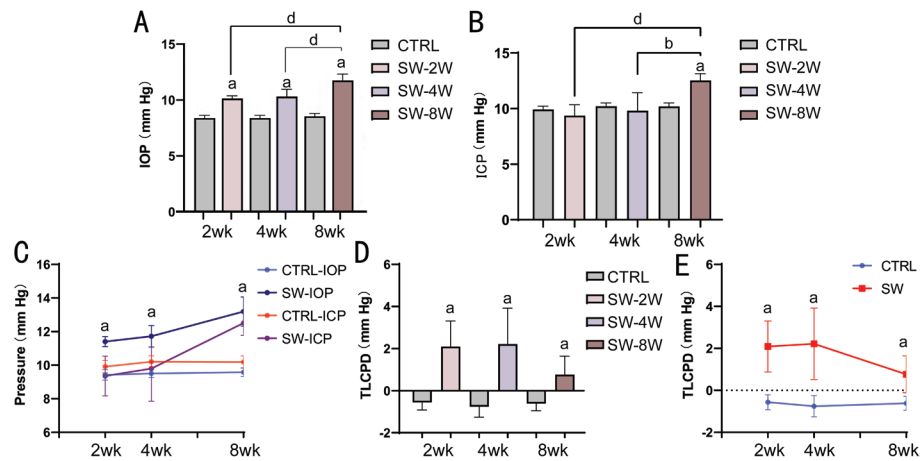


**Figure 2 IOP, ICP, and TLCPD in SW rats** A: IOP values in rats ( $n=12$ ); B: ICP values in rats ( $n=8$ ); C: Line graph depicting changes in IOP and ICP pressure. D: TLCPD results in SW rats ( $n=8$ ). E: Line graph showing TLCPD results in both SW and control rats ( $n=8$ ). <sup>a</sup> $P<0.05$  between the SW group and the control group at the same time point. <sup>b</sup> $P<0.01$ , <sup>c</sup> $P<0.001$ , <sup>d</sup> $P<0.0001$ . IOP: Intraocular pressure; ICP: Intracranial pressure; SW: Simulated weightlessness; TLCPD: Trans-lamina cribrosa pressure difference; CTRL: Control.

retinal RGCs and Iba-1-stained microglia. Fluorescence-positive cells were analyzed systematically to determine the extent of neural and immune changes under experimental conditions.

**Morphology Assessment of Microglia** Sholl analysis was employed to quantify the number of dendritic intersections at varying radial distances from the soma center<sup>[26-27]</sup>. Using the straight line tool in FIJI (Image J), a line was drawn from the center of the IBA cell to the longest branch. The IBA cells, stained with green fluorescence, were selected by using the Image>Color>Split Channels option. The IBA cell morphology was enhanced by applying the Process>Filters>Unsharp Mask and Noise>Despeckle options. Then, the image was converted to a black-and-white image (binary) using the Image>Adjust>Threshold option for fluorescence quantification. Finally, the mean branch length, max branch length, and number of branches were calculated using the neuroanatomy Shortcuts>Sholl Analysis>Legacy: Sholl Analysis (From image) option.

**Statistical Analysis** Statistical analyses were conducted using SPSS 27.0 (IBM, USA) with graphical representation generated in GraphPad Prism 9.0 (GraphPad Software, USA). Data distribution normality was verified through Shapiro-Wilk testing. Longitudinal effects of simulated microgravity were evaluated using one-way ANOVA across experimental timepoints (2wk, 4wk, 8wk). Post-hoc analysis employing Tukey's test identified specific temporal differences when ANOVA revealed significant effects. Between-group comparisons (control vs simulated microgravity) at individual timepoints utilized independent samples *t*-tests. For non-normally distributed data, nonparametric alternatives were implemented: Kruskal-Wallis test for multi-group comparisons and Mann-Whitney *U* test for pairwise analysis. All data are

expressed as mean±standard deviation (SD), with statistical significance threshold established at  $P<0.05$ .

## RESULTS

**Effects of Simulated Weightlessness in Tail Suspension on IOP, ICP, and TLCPD in Rats** we measured IOP and ICP in rats subjected to tail suspension for 2, 4, and 8wk. As delineated in Figure 2, SW induced differential pressure alterations in ocular. The control group maintained stable IOP levels throughout the experimental period (2wk:  $9.41\pm 0.28$  mm Hg; 4wk:  $9.38\pm 0.32$  mm Hg; 8wk:  $9.43\pm 0.25$  mm Hg). IOP exhibited immediate elevation across all SW groups compared with time-matched controls ( $P<0.05$ ) in Table 1. SW led to a clear, time-dependent elevation in IOP. In the SW-2W group, IOP increased significantly to  $11.41\pm 0.31$  mm Hg. With prolonged exposure, the SW-4W rats exhibited an IOP of  $11.72\pm 0.64$  mm Hg, and by 8wk, the SW-8W group reached an IOP of  $13.20\pm 0.87$  mm Hg.

Tukey's multiple comparisons confirmed that each group differed significantly from the others ( $P<0.01$ ), indicating a progressive rise in IOP with extended SW duration (Figure 2A). A delayed response in ICP was observed, with significant differences appearing only at the later experimental stages. ICP values in the control group remained stable throughout the study duration (2wk:  $9.88\pm 0.33$  mm Hg; 4wk:  $9.85\pm 0.29$  mm Hg; 8wk:  $9.90\pm 0.31$  mm Hg). The SW-2W group displayed ICP levels comparable to control-2W ( $9.35\pm 1.16$  mm Hg,  $P>0.05$ ), while the SW-4W group showed initial elevation ( $9.78\pm 1.92$  mm Hg vs CTRL-4W,  $P>0.05$ ). In the SW-8W group, ICP reached  $12.51\pm 0.74$  mm Hg, showing significant differences compared to both the SW-4W group ( $P<0.001$ ) and the control group ( $P<0.001$ ). These results demonstrate that SW leads to a significant, time-dependent increase in both IOP and ICP. The most significant ICP increase was observed in the SW-8W group

**Table 1** Experimental data of control group

Parameters	Control-2W		Control-4W		Control-8W	
	Mean±SD	95%CI	Mean±SD	95%CI	Mean±SD	95%CI
IOP (mm Hg)	9.43±0.31	9.23 to 9.62	9.5±0.24	9.35 to 9.65	9.58±0.26	9.42 to 9.75
ICP (mm Hg)	9.91±0.36	9.61 to 10.22	10.21±0.35	9.91 to 10.5	10.19±0.37	9.88 to 10.5
TLCPD (mm Hg)	-0.56±0.35	-0.86 to -0.27	-0.76±0.5	-1.18 to -0.34	-0.61±0.34	-0.9 to -0.33
PHNR (μV)	37.79±7.61	32.96 to 42.62	34.18±3.7	31.83 to 36.52	31.64±4.3	28.91 to 34.37
a-wave (μV)	46.11±9.4	40.13 to 52.08	42.02±3.54	39.77 to 44.26	38.88±4.69	35.9 to 41.86
b-wave (μV)	392.2±104.3	325.9 to 458.4	358.8±59.36	321.1 to 396.5	331.8±58.53	294.6 to 369
OMR (C/D)	0.5±0.06	0.46 to 0.54	0.49±0.03	0.48 to 0.51	0.49±0.03	0.47 to 0.5
OCT (μm)	218.5±7.67	213.7 to 223.4	216.2±10.08	209.8 to 222.6	213.7±9.91	207.4 to 220
NFL-GCL (μm)	28.69±5.66	25.09 to 32.28	28.22±3.53	25.98 to 30.47	27.25±3.46	25.05 to 29.45
INL (μm)	28.83±3.98	26.3 to 31.36	29.12±3.54	26.87 to 31.37	28.59±3.56	26.33 to 30.85
ONL (μm)	53.91±3.77	51.52 to 56.31	52.71±3.94	50.21 to 55.22	51.76±3.92	49.27 to 54.25
RGCs (cells/mm <sup>2</sup> )	250.1±47.07	218.5 to 281.7	255.9±43.48	228.3 to 283.5	252.2±42.87	224.9 to 279.4
Sholl max branch length (μm)	50.68±2.56	48 to 53.36	49.91±3.32	46.42 to 53.4	48.52±3.26	45.1 to 51.94
Sholl average branch length (μm)	10.61±0.69	9.89 to 11.34	12.19±0.85	11.29 to 13.08	11.84±0.85	10.94 to 12.73
Sholl number of branches (μm)	63.50±14.35	48.44 to 78.56	62.86±9.41	52.98 to 72.73	60.95±9.13	51.36 to 70.53

IOP: Intraocular pressure; ICP: Intracranial pressure; TLCPD: Trans-lamina cribrosa pressure difference; PhNR: Photopic negative response; NFL-GCL: Nerve fiber layer-ganglion cell layer complex thickness; INL: Inner nuclear layer thickness; ONL: Outer nuclear layer thickness; OCT: Optical coherence tomography; RGC: Retinal ganglion cell density. a-wave amplitude: Photoreceptor response (μV); b-wave amplitude: Bipolar cell response (μV); OMR: Optomotor response spatial frequency threshold [cycles per degree (C/D)].

(12.49±0.73 mm Hg vs CTRL-8W, *P*<0.01), with significant progression from the SW-4W group (*P*<0.01) The line graph depicting the changes in IOP and ICP over time illustrates the extent of their variations (Figure 2C).

Quantitative assessment of TLCPD revealed significant alterations under simulated microgravity conditions. The control group showed consistent and stable data, while the SW cohorts exhibited progressive pressure dysregulation, including a reversal in the direction of the TLCPD (Figure 2D, 2E). At the 2-week time point, the SW group demonstrated a significant positive shift to 2.09±1.22 mm Hg compared to the control group (*P*<0.05). This elevation reached its peak at 4wk (2.22±1.71 mm Hg vs CTRL, *P*<0.05), followed by partial normalization at 8wk (0.76±0.88 mm Hg, *P*<0.05).

**Visual Function Impairment in Tail-Suspended Rats: ERG and OMR** To evaluate the impact of simulated weightlessness on retinal function, we utilized ERG and optomotor response (OMR) spatial frequency analysis in rats exposed to simulated weightlessness for 2, 4, and 8wk (Figure 3A, 3B). The data of the control group are presented in Table 1, and the data of the SW experimental group are presented in Table 2. The results indicated a progressive decline in retinal function with increasing exposure time, with control groups maintaining stable physiological values throughout the study. In ERG testing, the PhNR amplitude was significantly reduced in the SW groups compared to controls, demonstrating a time-dependent decline in RGC function. the SW groups exhibited significant reductions at all timepoints (SW-2W: 25.33±9.81 μV;

SW-4W: 28.18±7.94 μV; SW-8W: 21.41±5.18 μV, *P*<0.01). The most pronounced reduction was observed at 8wk, with a 32.3% decrease compared to the control group (*P*<0.01; Figure 3F). For the a-wave amplitudes, which reflect photoreceptor activity, the control group exhibited a gradual decrease over time. Significant reductions in a-wave amplitude were only observed in the SW-4W (36.03±9.50 μV, *P*<0.05) and SW-8W (36.57±9.68 μV, *P*<0.05) groups, representing a 14.3% and 6.0% decrease compared to controls, respectively. The SW-2W group (36.93±10.26 μV) did not show a statistically significant difference (*P*>0.05), although the trend suggested early changes in retinal response. (Figure 3D). Regarding the b-wave amplitudes, which reflect bipolar cell activity, both the SW and control groups exhibited a decline over time. Control values decreased from 392.2±104.3 μV at 2wk to 331.8±58.53 μV at 8wk, while the SW groups showed significantly lower values at all timepoints (SW-2W: 337.5±92.13 μV; SW-4W: 269.5±74.99 μV; SW-8W: 277.8±75.17 μV, *P*<0.05). The most substantial reduction occurred at 4wk, with a 24.9% decrease compared to controls (*P*<0.01; Figure 3E). In the OMR analysis, the SW groups exhibited significant reductions starting at 4wk [SW-4W: 0.43±0.07 cyclers per degree (C/D); SW-8W: 0.40±0.05 C/D, *P*<0.05], representing a 12.2% and 18.4% decrease, respectively. The SW-2W group (0.47±0.08 C/D) did not show a statistically significant difference (*P*>0.05, Figure 3F). In summary, these results demonstrate a complex and progressive pattern of visual function impairment under SW, with

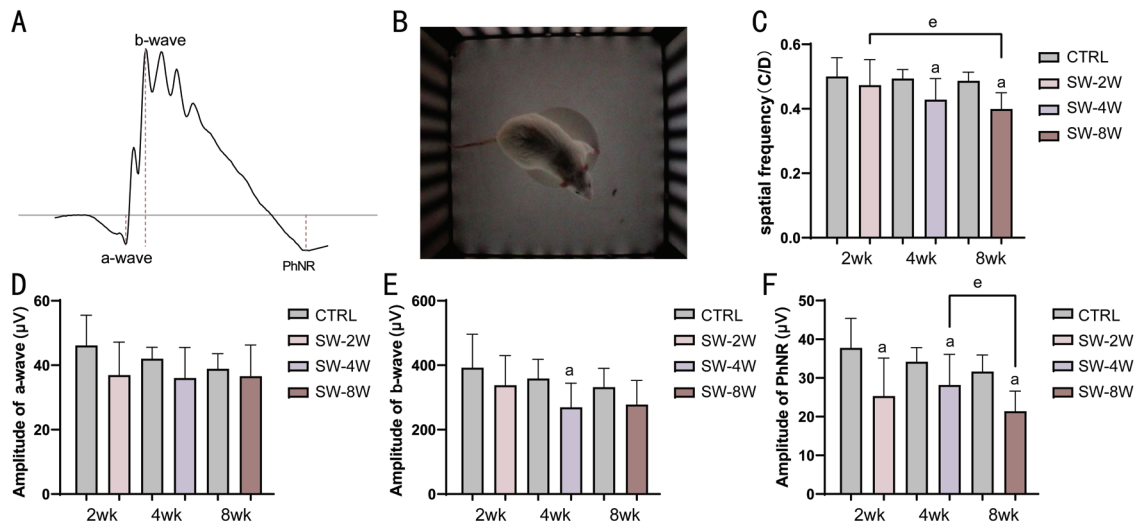


**Figure 3 Visual function assessment in SW rats** A: Schematic representation of the a-wave, b-wave, and PhNR waveforms in ERG response; B: OMR test conducted on rats in a darkroom; C: Spatial frequency contrast sensitivity (C/D) derived from OMR testing in SW rats; D: a-wave in the ERG of SW rats; E: b-wave in the ERG of SW rats; F: PhNR wave in the ERG of SW rats, <sup>a</sup>*P*<0.05 (*n*=12), <sup>a</sup>*P*<0.05 between the SW group and the control group at the same time point. ERG: Electroretinogram; OMR: Optomotor response; SW: Simulated weightlessness; PhNR: Photopic negative response; CTRL: Control.

**Table 2 Experimental data statistics in rats subjected to SW**

Parameters	SW-2W		SW-4W		SW-8W	
	Mean±SD	95%CI	Mean±SD	95%CI	Mean±SD	95%CI
IOP (mm Hg)	11.41±0.31	11.21 to 11.6	11.72±0.64	11.29 to 12.15	13.2±0.87	12.58 to 13.82
ICP (mm Hg)	9.36±1.18	8.37 to 10.35	9.8±1.95	8.17 to 11.42	12.51±0.74	11.89 to 13.13
TLCPD (mm Hg)	2.09±1.22	1.08 to 3.11	2.22±1.71	0.79 to 3.64	0.76±0.88	0.03 to 1.5
PHNR (μV)	25.33±9.81	17.13 to 33.52	28.18±7.94	23.14 to 33.22	21.41±5.18	18.11 to 24.7
a-wave (μV)	36.93±10.26	28.35 to 45.5	36.03±9.5	29.99 to 42.06	36.57±9.68	30.42 to 42.72
b-wave (μV)	337.5±92.13	260.5 to 414.5	269.5±74.99	221.8 to 317.1	277.8±75.17	230.1 to 325.6
OMR (C/D)	0.47±0.08	0.42 to 0.53	0.43±0.07	0.38 to 0.47	0.4±0.05	0.36 to 0.44
OCT (μm)	226.3±8.96	219.9 to 232.7	229.2±3.85	226.7 to 231.6	215.9±4.57	213 to 218.8
NFL-GCL (μm)	30.85±6.41	26.26 to 35.44	34.66±3.7	32.31 to 37.01	27.26±4.17	24.61 to 29.9
INL (μm)	28.66±3.47	26.18 to 31.14	31.96±2.87	30.14 to 33.78	30.64±3.91	28.16 to 33.12
ONL (μm)	53.43±4.03	50.55 to 56.32	48.57±3.01	46.66 to 50.48	39.39±3.17	37.37 to 41.4
RGCs (cells/mm <sup>2</sup> )	236.5±46.21	205.4 to 267.5	223.4±20.29	209.7 to 237	199.6±42.43	171.1 to 228.1
Sholl max branch length (μm)	46.53±2.72	43.68 to 49.39	44.98±2.14	42.73 to 47.23	43.17±3.13	39.88 to 46.45
Sholl average branch length (μm)	9.10±0.69	8.37 to 9.83	9.00±2.08	6.82 to 11.18	8.30±0.72	7.54 to 9.06
Sholl number of branches (μm)	38.67±8.94	29.29 to 48.05	33.67±5.92	27.45 to 39.88	28.50±7.97	20.14 to 36.86

SW: Simulated weightlessness; IOP: Intraocular pressure; ICP: Intracranial pressure; TLCPD: Trans-lamina cribrosa pressure difference; PhNR: Photopic negative response; NFL-GCL: Nerve fiber layer-ganglion cell layer complex thickness; INL: Inner nuclear layer thickness; ONL: Outer nuclear layer thickness; OCT: Optical coherence tomography; RGC: Retinal ganglion cell density. a-wave amplitude: Photoreceptor response (μV); b-wave amplitude: Bipolar cell response (μV); OMR: Optomotor response spatial frequency threshold [cycles per degree (C/D)].

different components of the retinal response (PhNR, a-wave, B-wave, and OMR) exhibiting varying degrees of sensitivity to microgravity exposure. Ganglion cell function appeared to be particularly vulnerable to SW, with early and sustained reductions in PhNR amplitude, while other retinal responses showed more delayed but significant declines.

**In vivo Retinal Thickness Measurement in Tail-Suspended Rats: OCT** In the short-term microgravity groups (2 and

4wk), an increase in total retinal thickness was observed. The data of the control group are presented in Table 1, and the data of the SW experimental group are presented in Table 2. Specifically, the average retinal thickness in the SW-2W group was 226.3±8.96 μm, and in the SW-4W group, it was 229.2±3.85 μm, both significantly higher than that of the control group (SW-4W: 216.2±10.08 μm; Figure 4A). However, after 8wk of microgravity exposure, the retinal

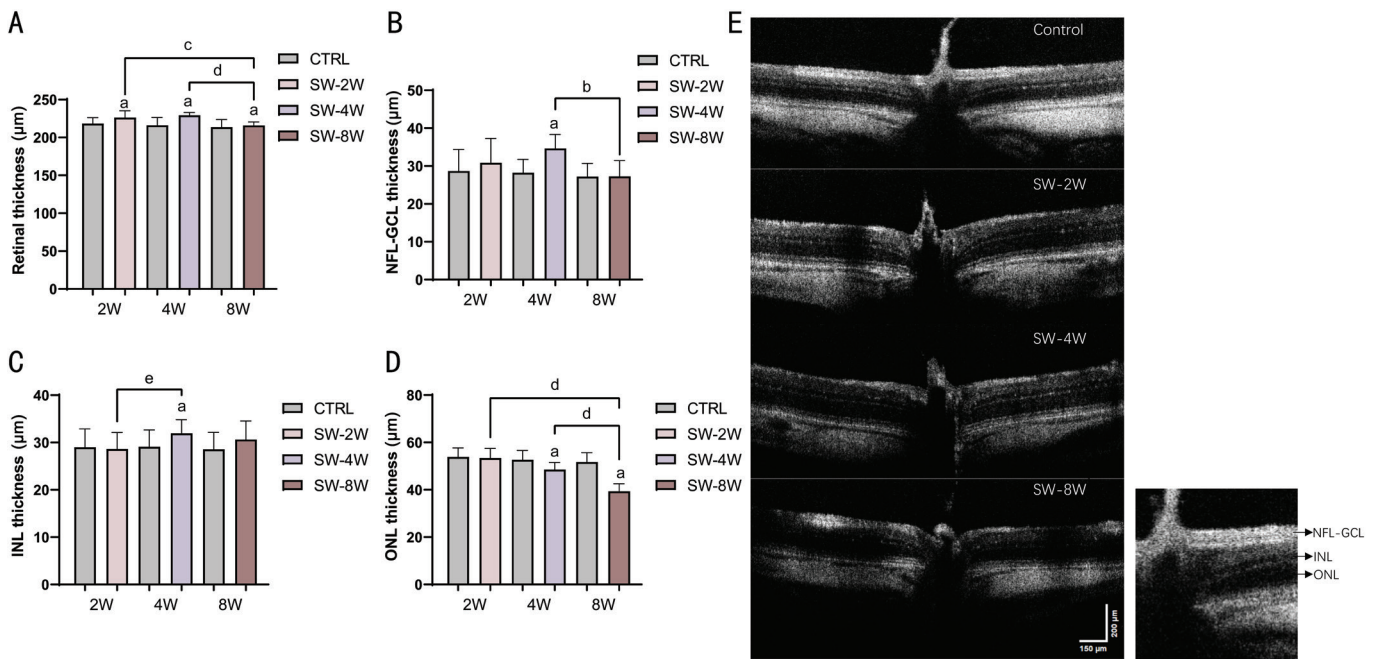


**Figure 4 Retinal thickness measurements in SW rats using OCT** A: Full retinal thickness (μm); B: NFL-GCL thickness (μm); C: INL thickness (μm); D: ONL thickness (μm); E: OCT image of the retina in rats. <sup>a</sup>*P*<0.05 between the SW group and the control group at the same time point. <sup>e</sup>*P*<0.05, <sup>b</sup>*P*<0.01, <sup>c</sup>*P*<0.001, <sup>d</sup>*P*<0.0001 (*n*=12). OCT: Optical coherence tomography; INL: Inner nuclear layer; NFL-GCL: Nerve fiber layer and ganglion cell layer complex; ONL: Outer nuclear layer; SW: Simulated weightlessness; CTRL: Control.

thickness in the SW-8W group decreased to 215.9±4.57 μm, which was significantly different from the SW-2W and SW-4W groups (*P*<0.01). Regarding the NFL-GCL complex thickness (Figure 4B), the average thickness in the SW-2W group was 30.85±6.41 μm, and it significantly increased to 34.66±3.70 μm in the SW-4W group; in contrast, the SW-8W group showed a significant reduction to 27.26±4.17 μm compared with the SW-4W group (*P*<0.01). These findings suggest that short-term microgravity exposure may induce edema or compensatory thickening, whereas prolonged exposure results in atrophy. In the mid-term microgravity group, the INL thickness increased to 31.96±2.87 μm at 4wk, which was significantly higher than that in the SW-2W group (*P*<0.05); the control group (SW-4W) had an average INL thickness of 29.12±3.54 μm, with a significant difference observed only in the SW-4W group (*P*<0.05), while other comparisons showed no statistical difference (Figure 4C). For the ONL thickness, no significant changes were observed in the 2-week and 4-week exposure groups; however, the long-term microgravity group (8wk) demonstrated a significant decrease in ONL thickness to 39.39±3.17 μm compared with the control group (SW-8W: 51.76±3.92 μm), with significant differences relative to the SW-2W and SW-4W groups (*P*<0.001; Figure 4D). These results indicate that prolonged exposure to simulated microgravity may lead to degeneration or thinning of the outer retinal layers, as evidenced by the reductions in overall retinal thickness and the NFL-GCL complex, most notably in the ONL. whereas the INL thickness remained stable or even slightly increased relative to the control.

**Effects of Simulated Weightlessness on Retinal Morphology in Rats** In rats exposed to simulated microgravity for 2, 4, and 8wk (Figure 5A–5D), fundus imaging revealed no obvious retinal lesions. The data on retinal thickness in the control group are presented in Table 1, and the data on retinal thickness in the SW experimental group are presented in Table 2. At 2 and 4wk, the retinal architecture was preserved, with only slight alterations in vascular density and a marginal decrease in choroidal filling, particularly evident at 4wk. By 8wk, although the retinal vascular morphology remained normal, choroidal vascular filling was significantly reduced, indicating mild hemodynamic changes. These findings suggest that prolonged simulated microgravity may impair choroidal perfusion without causing overt retinal damage. In the hematoxylin-eosin (HE)-stained sections, we focused on the INL and ONL, which correspond to the damages observed in ERG and OCT. The retinal tissue in the control group exhibited normal structural integrity, with no apparent inflammation or abnormalities. In the 2-week simulated microgravity group, no significant differences in retinal layer thickness or cellular arrangement were observed (Figure 5E, 5F). In contrast, the SW-4W group showed a marked thickening of the NFL-GCL complex, which was consistent with the OCT measurements. Near the optic disc, the INL displayed mildly disorganized cellular arrangement, with arrows indicating areas of pronounced disorganization and thinning—possibly reflecting regional variations not captured by OCT—while the ONL exhibited only slight loosening of cells without significant

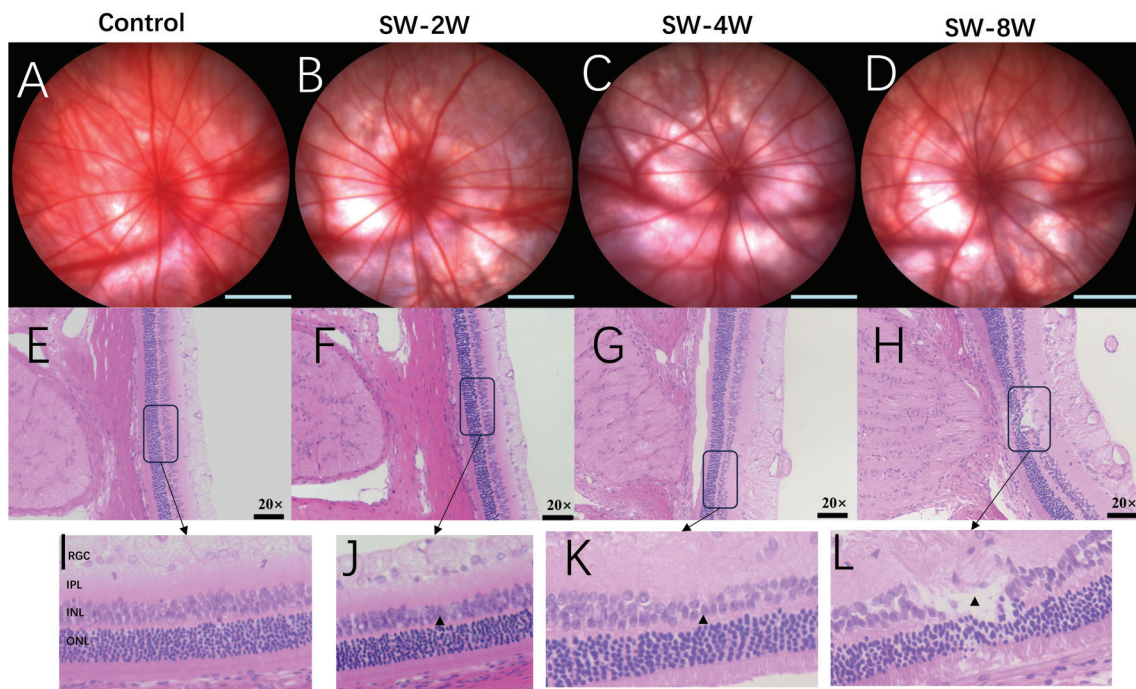


**Figure 5** *In vivo* fundus imaging and H&E-stained retinal sections of rats under SW A–D: Fundus photographs from each experimental group ( $n=12$  eyes per group/time point); E–H: Representative H&E -stained retinal sections from all groups; I–L: Regions outlined in black indicate the areas where retinal structures were analyzed ( $n=3$  eyes per group/time point). H&E: Hematoxylin-eosin; RGC: Retinal ganglion cell layer; IPL: Inner plexiform layer; INL: Inner nuclear layer; ONL: Outer nuclear layer; SW: Simulated weightlessness.

changes (Figure 5G, 5K). In the SW-8W group, retinal cells began to show irregular arrangements; the ganglion cell layer (GCL) became disorganized, with some cells exhibiting vacuolar degeneration, and the INL displayed a chaotic cellular arrangement (with arrow-indicated areas showing pressure-induced inward collapse), while the ONL cells appeared dispersed (Figure 5H, 5L). Overall, we observed that both the INL and ONL were affected as the duration of microgravity exposure increased. These morphological findings are largely consistent with the visual function changes observed in ERG and the *in vivo* retinal alterations detected by OCT.

**RGC Counting in Simulated Weightlessness Rats** To evaluate the potential impact of SW on RGCs, we prepared retinal flatmounts and performed RBPMS immunofluorescence staining (Figure 6A–6D). Non-overlapping images were captured in specific regions of the retina for quantitative analysis using Image J software. The analysis revealed a slight decrease in the number of RGCs in the SW groups, particularly with prolonged exposure. The study assessed the effects of different durations of SW (2, 4, and 8wk) on RGC count in rat retinas. The data on the count of retinal RGCs in the control group are presented in Table 1, and the data on retinal RGCs in the SW experimental group are presented in Table 2. The results showed no significant differences in the RGC count between the SW-2W and SW-4W groups compared to the control group. Specifically, the RGC counts were  $250.1 \pm 47.07$  and  $236.5 \pm 46.21$  for the SW-2W and SW-

4W groups, respectively, versus  $218.5 \pm 7.67$  in the control group ( $P=0.8634, 0.4909$ ). However, in the SW-8W group, the RGC count significantly decreased to  $200.3 \pm 40.53$ , which was notably lower than the control group ( $P=0.0295$ ). Tukey's multiple comparison analysis confirmed that the difference in RGC count between the SW-8W and control groups was statistically significant ( $P<0.05$ ). These findings suggest that prolonged exposure to SW, particularly after 8wk, results in significant damage to RGCs, with the most pronounced reduction in cell number observed in the 8-week exposure group (Figure 6N).

**Activation of Astrocytes in Retinal Neuroinflammation Under Simulated Weightlessness** Under SW conditions, astrocyte activation in the rat retina is a critical step in the pressure-related loss of retinal RGCs. The interaction between astrocytes and RGCs is considered an important indicator of changes in the IOP gradient. In the SW-2W group, immunofluorescence results showed slight thickening of the astrocyte processes, with a mild increase in branching and a slight upregulation of GFAP expression compared to the control group. These findings suggest that astrocytes may be in a mild reactive proliferation state, with early protective mechanisms being activated. By the SW-4W group, immunofluorescence showed significant thickening of astrocyte processes, with notable increases in branching and a significant rise in GFAP expression. This indicates that the degree of reactive proliferation has peaked, potentially

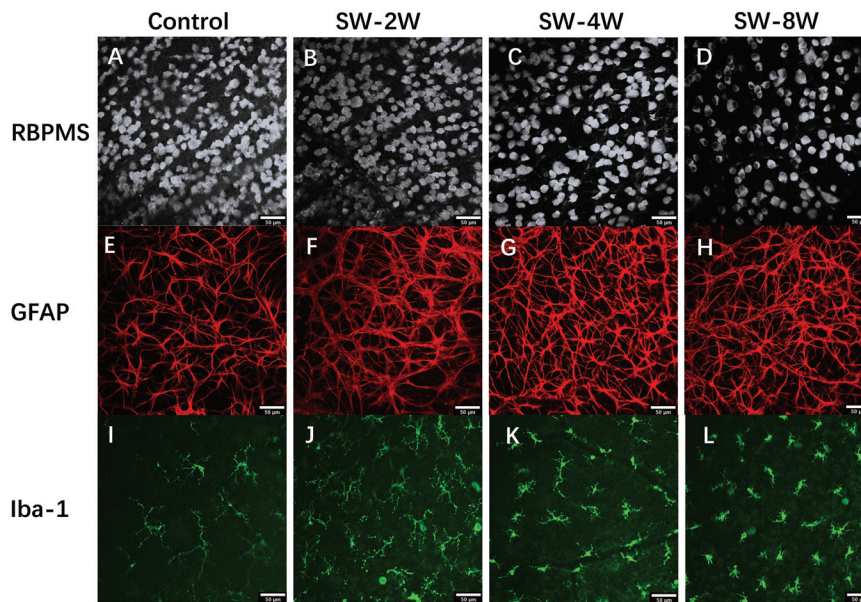


**Figure 6 Immunofluorescence analysis of retinal changes in rats under SW** A–D: Representative retinal flatmount images demonstrating RBPMS immunostaining (gray) for RGCs at 2, 4, and 8wk post-modeling, along with quantitative analysis of RGC numbers ( $n=11$  eyes per group/time point); E–H: Representative retinal flatmount images illustrating GFAP immunostaining (red) at 2, 4, and 8wk post-modeling ( $n=3$  eyes per group/time point); I–L: Representative images of Iba-1 immunostaining (green) in retinal flatmounts at 2, 4, and 8wk post-modeling, with quantification of microglia density ( $n=6$  eyes per group/time point). RGC: Retinal ganglion cells; SW: Simulated weightlessness; RBPMS: RNA-binding protein with multiple splicing; GFAP: Glial fibrillary acidic protein.

contributing to inflammation and the regulation of the BRB. In the SW-8W group, immunofluorescence results revealed a disordered structure of astrocyte processes, with sustained high GFAP expression. This indicates that while astrocyte activation remained at a high level, functional impairment might be occurring, which could further exacerbate the loss of RGCs (Figure 6A–6D).

**Microglial Activation in Retinal Inflammation Under Simulated Weightlessness** Microglial cell activation is closely associated with retinal degeneration. Immunofluorescence results showed that the number of microglial cells significantly increased in the SW-4W and SW-8W groups, accompanied by marked morphological changes characterized by a reduction in overall cell body size and a gradual enlargement and rounding of the nucleus. These changes indicate a transition from a resting to an activated state (Figure 6I–6L). The data of each index from the Sholl analysis of retinal microglia in the control group are presented in Table 1, and the data from the Sholl analysis of retinal microglia in the SW experimental group are presented in Table 2. To further explore the immunological characteristics at different time points, we employed Image J to perform Sholl analysis on retinal flat mounts from rats exposed to simulated microgravity, investigating the morphology and molecular activation of microglial cells. The results revealed a significant increase in IBA-1 positive microglial cells. Immunofluorescence observations demonstrated that, compared with the SW-2W group, microglial cells in the SW-

4W and SW-8W groups exhibited an amoeboid morphology—characterized by a rounder and larger cell body, reduced branching, and a tendency for the processes to retract toward the cell center. We further conducted skeleton analysis to evaluate the number of intersections at various radial distances from the cell body (Figure 7A). The analysis indicated that, compared to the control group, the number of intersections in microglial cells from the simulated microgravity groups was significantly reduced. Specifically, at 2wk, the number of intersections at different distances from the cell body was similar; however, at 4wk, the number of intersections remained at a low level. By 8wk, the number of intersections exhibited increased branching (Figures 7B–7D). Additionally, quantitative measurements from the skeleton analysis showed that the SW-4W and SW-8W groups had fewer branches and a shorter average branch length ( $P<0.05$ ). Further skeleton analysis revealed that the morphological changes in activated microglial cells in the simulated microgravity rat model were more pronounced compared with the control ( $P<0.05$ ; Figure 7E–7G). Collectively, these results indicate that under simulated microgravity, the microglial cells in the rat retina are significantly activated and undergo substantial morphological and functional alterations.

## DISCUSSION

During spaceflight, astronauts experience significant changes in the structure and function of multiple body systems, including blood shift towards the head, adaptive cardiovascular

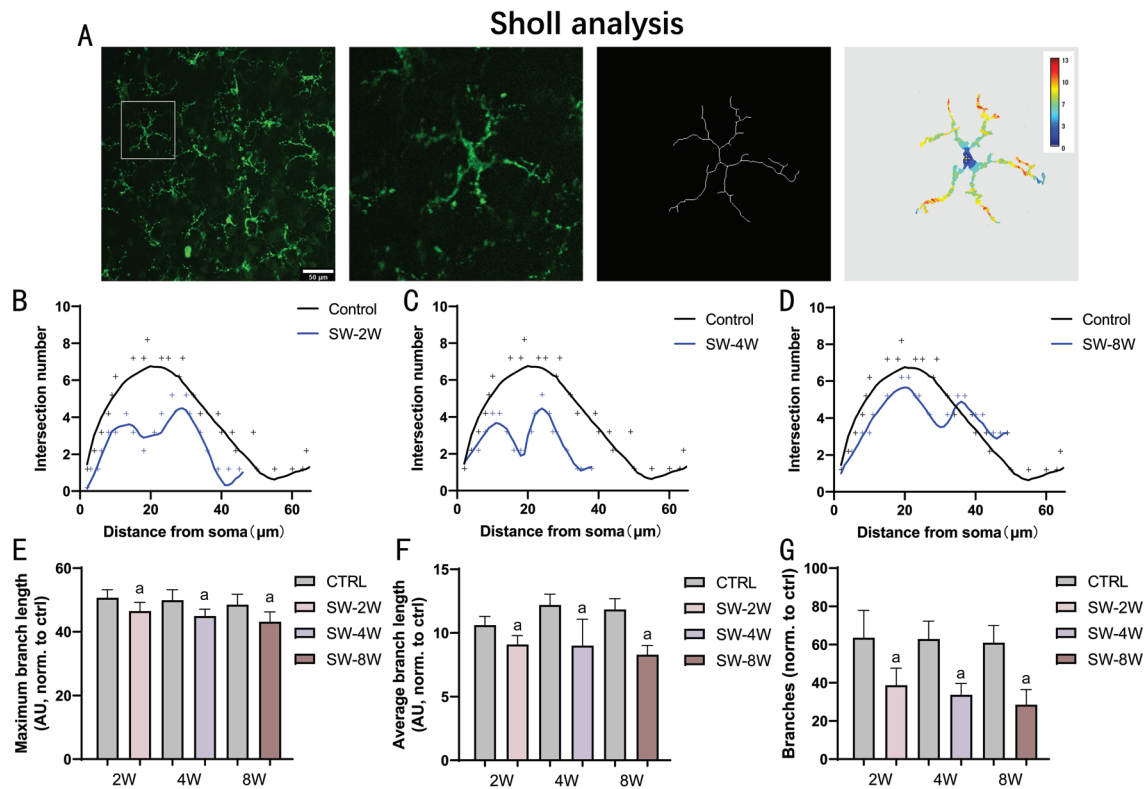


**Figure 7 Activation and morphological changes of retinal microglia in rats under SW** A: Representative images of Iba-1 staining were converted to binary format for Sholl analysis, and the resulting Sholl profiles for rats exposed to SW at 2, 4, and 8wk are presented ( $n=6$  eyes per group/time point); B–D: Skeleton analysis was used to quantify the number of intersections across groups; E: Maximum branch length; F: Average branch length; G: Total branch number were quantified. <sup>a</sup> $P<0.05$  between the SW group and the control group at the same time point. SW: Simulated weightlessness; CTRL: Control.

adjustments, and alterations in skeletal and muscular systems. These changes may affect astronauts' physical and mental health both during spaceflight and after returning to Earth<sup>[28]</sup>. Research has shown that acute IOP increase in a microgravity environment is associated with choroidal congestion<sup>[6]</sup>. However, sustained increased scleral venous pressure leads to reduced aqueous humor outflow, which is the primary cause of prolonged elevated IOP<sup>[29]</sup>. In our experiment, at two weeks of tail suspension, the IOP showed only a slight upward trend, and at four weeks, it remained stable. However, at the end of the experiment, there was a noticeable increase in IOP, with an overall upward trend. The IOP of the simulated microgravity group was significantly higher than that of the control group, although the difference was statistically significant, it remained within the normal range. This trend of IOP changes is similar to that observed in spaceflight and head-down tilt studies of simulated microgravity<sup>[6]</sup>. However, whether prolonged microgravity leads to irreversible pathological IOP elevation, and whether there exists a critical time point for pathological increases, remains to be further explored in future studies. In the case of fluid redistribution towards the head, the volume of blood and CSF in the brain increases, with blood shifting from the lower body to the head, leading to head venous congestion,

increased vortex vein pressure, and stagnation of choroidal blood flow. The resulting congestion and dilation ultimately lead to choroidal thickening<sup>[30]</sup>. Changes in ICP could result in optic nerve damage and damage at the lamina cribrosa. Increased ICP and CSF may cause the optic nerve sheath to dilate, thereby compressing the optic nerve. Furthermore, the swelling of myelinated axons and increased myelin thickness may be related to insufficient nutritional support from oligodendrocytes<sup>[31]</sup>. We measured the ICP of rats in the simulated microgravity condition, and the overall trend was somewhat different from our expectations. The overall change in ICP was relatively low, with a significant increase only at 8wk, which was statistically different. Lee *et al*<sup>[32]</sup> reported that several astronauts with prominent optic disc edema underwent lumbar punctures at 12 and 57d after returning to Earth, with ICP values of 28 and 28.5 cm H<sub>2</sub>O, respectively. At 19 and 66d post-return, their ICP values were 21 and 22 cm H<sub>2</sub>O, respectively. Microgravity leads to fluid redistribution, and as a portion of circulating blood shifts from the lower body to the upper body, the perfusion pressure in the head increases by 20–30 mm Hg<sup>[13]</sup>. In the study by Kergoat and Durand<sup>[33]</sup>, relatively short exposure to microgravity led to retinal ischemia. Retinal cells are more sensitive to ischemia

than other retinal cells<sup>[34]</sup>, and prior studies have reported that long-term spaceflight leads to abnormal volumes of gray matter, white matter, and CSF<sup>[35]</sup>. Therefore, the effects of simulated microgravity on intracranial blood vessels may play a crucial role in the pathological process of elevated ICP. Conversely, elevated ICP can lead to optic nerve lesions and even the development of ocular diseases<sup>[36]</sup>. Although the changes in ICP were subtle, by combining them with IOP data, we further analyzed the alterations in the TLCPD. The latest method for measuring ICP employs an implantable wireless pressure telemetry system based on a small, low-pressure sensor positioned in the lower temporal lobe. The telemetry sensor is placed in the anterior chamber for IOP measurement and in the brain parenchyma at the level of the eye to monitor ICP. This approach enables long-term, real-time monitoring of ICP changes, and its reliability has been confirmed by Jasien *et al*<sup>[37]</sup>. Additionally, our current ICP measurements are obtained from the CSF pressure of rats under deep anesthesia—a condition that may be influenced by factors such as physical activity and body positioning. Wireless remote pressure sensing will become an important direction in our research on the TLCPD.

TLCPD and its impact on rat optic nerve health under simulated microgravity conditions have not been fully studied. TLCPD refers to the difference between IOP and ICP, playing a crucial role in the biomechanical properties of the optic nerve head and optic nerve damage (Figure 8)<sup>[21]</sup>. The optic nerve, a white matter tract of the central nervous system, is ensheathed by all three meningeal layers and surrounded by CSF in the subarachnoid space (SAS)<sup>[37]</sup>. Therefore, in addition to IOP, the optic nerve is also exposed to ICP. The lamina cribrosa separates these two pressurized regions. The difference between the posteriorly directed IOP and the anteriorly directed ICP is known as the TLCPD<sup>[38]</sup>.

The rat optic nerve head differs from those of humans and non-human primates in that it lacks the collagenous lamina cribrosa, but has a similar structure derived from astrocytes<sup>[39]</sup>. Additionally, the blood supply to the rat optic nerve head is derived from the central retinal artery without contributions from the choroid<sup>[40]</sup>. Despite these anatomical differences, it appears that certain relationships predicted by the rise of IOP and ICP are preserved in mice, at least to some extent. This is an important finding that supports the continued use of mice as a key model for simulated microgravity research. Previous studies have indicated that simulated microgravity may lead to demyelination and activation of glial cells in the rat brain, suggesting potential effects on the nervous system<sup>[41-42]</sup>. However, direct evidence regarding the specific impact of simulated microgravity on TLCPD is lacking. Our previous research showed that RGCs in low ICP rats have

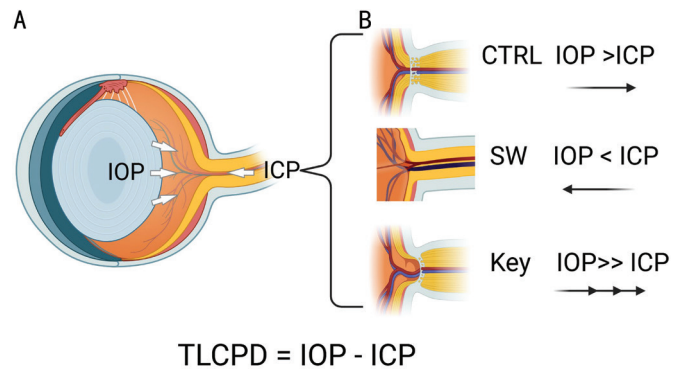


**Figure 8 Schematic of TLCPD** TLCPD is defined as the difference between IOP and ICP. Under normal conditions, IOP exceeds ICP, resulting in a pressure gradient directed toward the posterior of the eyeball. Under SW, the pressure gradient is reversed, pointing toward the anterior of the eyeball. In special cases, such as glaucoma—where IOP is substantially higher than ICP—the resulting large pressure gradient is directed toward the posterior of the eyeball. TLCPD: Trans-lamina cribrosa pressure difference; IOP: Intraocular pressure; ICP: Intracranial pressure; SW: Simulated weightlessness.

functional and morphological damage<sup>[22,43]</sup>. However, the potential retinal immune characteristics of ICP changes and RGC damage remain unclear. We previously established a low ICP rat model induced by decreasing the translaminal pressure difference, and a series of experiments confirmed its reliability and effectiveness<sup>[44-45]</sup>. This has provided us with significant insights. Our study suggests that the changes induced by microgravity in this pressure gradient may contribute to the observed retinal alterations. At two weeks, we observed a significant positive shift in TLCPD in the simulated microgravity group (SW-2W), which continued to increase at four weeks (SW-4W) and maintained this trend at eight weeks (SW-8W). This indicates that during exposure to simulated microgravity, the physiological pressures governing the ocular environment changed (both in magnitude and direction), and these changes persisted over time. Our analysis suggests that although the numerical changes in TLCPD are less significant in terms of their pathological effects, the alteration in the direction of the pressure gradient appears to have a more profound impact. It is possible that with prolonged tail suspension, the TLCPD may continue to increase in value, which will become a focus of our subsequent research.

Through immunofluorescence staining of retinal flat mounts in rats, we observed changes in three indicators. First, the number of RGCs showed a downward trend with prolonged exposure to microgravity, with significant differences observed only in the 8-week group. Short-term microgravity damage may not directly reflect RGC loss, but over time, damage gradually worsens, and RGCs undergo apoptosis due to the pressure changes mentioned above, consistent with the PhNR

results obtained in ERG. Previous research by Zhao *et al*<sup>[46]</sup> found that microgravity in rats can lead to optic nerve damage and apoptosis of RGCs based on the simulated microgravity model, we analyzed the immune cells in rats. We observed significant activation of microglial cells and astrocytes, along with morphological and molecular changes in the retina. Microglial cells, as resident immune cells, are the first line of defense in a healthy retina<sup>[47]</sup>. Activation of microglial cells signifies the development of various inflammatory diseases, and microglia-mediated inflammation typically leads to neuronal damage<sup>[48]</sup>. We labeled Iba1, a specific marker for microglial cells<sup>[49]</sup>, to determine whether optic nerve damage in rats under long-term simulated microgravity is associated with this inflammatory response. Literature records that activated microglial cells can undergo pro-inflammatory M1 polarization and anti-inflammatory M2 polarization depending on the situation. When demyelinating lesions occur, the anti-inflammatory M2 phenotype predominates 3–10d later, playing a role in debris clearance, tissue remodeling, and repair<sup>[48,50-52]</sup>. Long-term tail suspension simulating microgravity induces microglial-mediated inflammation and demyelination in the optic nerve, with a trend toward gradual spread. Future studies should further label M2 macrophage subtypes to identify the repair phase of the damage. Astrocytes, which are widely distributed and respond rapidly, play a significant role in the survival or death of retinal RGCs under microgravity. They are also critical for maintaining the BRB, modulating neuroinflammation, promoting neuronal survival, and facilitating phagocytosis. The complex crosstalk between microglial cells and astrocytes can fine-tune immune responses in retinal diseases, that excessive immune activation could trigger cell apoptosis and inflammation—findings that are consistent with previous studies on retinal changes in mice after long-term spaceflight<sup>[53]</sup>.

Under simulated microgravity conditions, we employed non-invasive retinal light reflex OMR and flash ERG to monitor retinal function in rats. In OMR behavioral tests, spatial frequency contrast sensitivity exhibited significant differences between the 4-week and 8-week groups. During the experiment, we observed that rats under simulated microgravity conditions exhibited sluggish responses and slow activity upon initially entering the testing environment. In the first 15min, it was difficult to obtain accurate measurements of contrast sensitivity; however, by extending the testing period to 30min, stable measurements were achieved. From a behavioral perspective, this indirectly reflects the damage caused by SW. The outer retina in mammals primarily consists of rod and cone photoreceptors, whose expression of photopigments (rhodopsin for rods and opsins for cones) is closely related to retinal physiological function and ERG results. Flash ERG

sensitively and objectively reflects the overall function of the retina, recording the electrical responses from both neuronal and non-neuronal cells in the retina after light stimulation. In our experiment, a flash ERG stimulus of 3.0 cd·s/m<sup>2</sup> was used to record the amplitudes of the a-wave, b-wave, and PhNR. Changes in the amplitudes of the a-wave, b-wave, and PhNR are related to structural changes in retinal layers: the a-wave primarily reflects dysfunction in the ONL, the b-wave is associated with abnormalities in the INL, and the PhNR indicates damage to retinal RGCs and the NFL. The results showed that the a-wave amplitude decreased similarly in the 2-, 4-, and 8-week groups, but this change was not statistically significant. In contrast, the b-wave amplitude exhibited a slight decline at 2wk, a significant decrease at 4wk, and a slight rebound at 8wk; compared with the control group, only the 4-week group showed a statistically significant difference ( $P<0.05$ ). The PhNR amplitude exhibited a significant decline at 8wk ( $P<0.05$ ), and overall, a downward trend was observed that reached statistical significance ( $P<0.01$ ). In our study, significant changes in ERG waveform were observed under prolonged simulated microgravity, which is consistent with fluctuations in ERG amplitude observed in other head-down tilt animal models and even in humans<sup>[32,54-55]</sup>. These results confirm functional damage to vision and apoptosis of RGCs under simulated microgravity. Our findings are consistent with histological damage. Functionally, previous studies have suggested that blood circulation in the inner retina influences inhibitory feedback loops and their signal transmission<sup>[56]</sup>. In the study by Dai *et al*<sup>[57]</sup>, they measured the ERG of mice under weightlessness and suggested that short-term exposure to microgravity could affect the ERG and retinal microcirculation, but did not result in significant permanent retinal damage. However, the impact of simulated microgravity on retinal blood circulation requires further investigation to gain a deeper understanding of its mechanisms.

Progressive changes in TLCPD may exacerbate retinal ischemia, further impairing retinal function. The temporal pattern observed in TLCPD aligns with retinal function changes measured by ERG and OMR. For example, a significant reduction in PHNR amplitude was noted starting at the two-week time point, indicating a decline in RGC activity potentially attributed to changes in the trans-lamina cribrosa pressure gradient. Over time, the amplitudes of the b-wave and a-wave also gradually decreased, further supporting the hypothesis that mechanical changes in TLCPD may affect retinal neural pathways. Significant reductions in retinal function observed after four and eight weeks of exposure to simulated microgravity reflect the complex effects of pressure dysregulation and may help explain the observed increases in retinal structure and function under prolonged microgravity

exposure. This is particularly important under microgravity conditions, as the redistribution of body fluids increases the load on the layer<sup>[46]</sup>. A recent study using mathematical modeling reported changes in the venous function of the eye under simulated microgravity, where the central retinal vein passes through all layers of the retina, and the effects of microgravity on this layer could lead to changes in retinal venous or microcirculatory hemodynamics<sup>[58]</sup>. In the International Space Station (ISS) or during spaceflight, the environmental impacts are more complex than the simulated microgravity on Earth<sup>[59-60]</sup>. Although part of the animal's body is suspended, the forelimbs remain in contact with the ground. However, under true microgravity conditions, the entire body floats weightlessly<sup>[61]</sup>. These studies have shown that 35d of spaceflight induce apoptosis of retinal endothelial cells, potentially disrupting the integrity of the BRB and leading to changes in the expression of proteins involved in cell death, cell cycle, immune response, mitochondrial function, and metabolic stress, which result in more widespread changes in ocular structure and function<sup>[12]</sup>.

We used OCT to measure the retinal thickness 200  $\mu\text{m}$  from the optic disc center in long-term tail-suspended rats. The results showed that the overall retinal thickness in the simulated microgravity group became thinner with prolonged suspension time. Previous studies have reported an increase in retinal thickness<sup>[62]</sup>, which we believe could be attributed to edema and other factors in the short-term microgravity, while longer suspension periods manifested as histological damage. We further subdivided the retina into three layers: the thickness of the nerve fiber layer and NFL-GCL, the INL, ONL and the overall retinal thickness. Our measurements showed that the thickness of the INL-GCL complex demonstrated a trend consistent with the overall retinal thickness, with statistical differences ( $P < 0.05$ ), showing a noticeable thinning at 8wk. In contrast, the thickness of the INL showed only a slight increase in the 2-week and 4-week groups, with a reduction to control levels at 8wk, showing no statistical difference ( $P < 0.05$ ). However, recent studies have reported a decrease in retinal and choroidal thickness in mice after 35d of spaceflight at 10wk of age<sup>[59]</sup>. In a recent study by Mu *et al*<sup>[63]</sup>, OCT measurements of rats exposed to simulated microgravity also revealed thinning of the retinal ONL layer, similar to our findings. This suggests the impact of microcirculation on tissue homeostasis. In the HE-stained sections, we observed that the retinal structure in the control group was intact with no apparent inflammation; in the 2-week group, the thickness and cellular arrangement of all layers were essentially normal. In the 4-week group, the NFL-GCL complex was markedly thickened (consistent with OCT results), and near the optic disc, the INL showed slight disorganization and localized thinning, with the ONL cells

appearing slightly loosened. In the 8-week group, the retinal cells exhibited irregular arrangement, the ganglion cell layer was disorganized, some cells showed vacuolar degeneration, the INL displayed pressure-induced inward collapse, and the ONL cells were dispersed. Overall, as the duration of microgravity exposure increased, both the INL and ONL were affected, which is consistent with the retinal functional changes observed in ERG and OCT. Our results are similar to the HE-stained section damage observed in the studies by Mu *et al*<sup>[63]</sup> and Li *et al*<sup>[54]</sup>, but our findings are more severe. This may be related to the duration of the model.

We used rats exposed to simulated microgravity and a control group. Initially, we analyzed changes in IOP and ICP, and calculated the TLCPD. Then, we assessed retinal function damage in rats using OMR and flash ERG. We also measured the number of retinal RGCs and the morphology and function of microglial cells and astrocytes. Our findings suggest that this mechanism may involve excessive activation of pressure-induced neuroimmune cells, leading to chronic loss of RGCs. However, compared to rats with long-term tail suspension, the visual function damage caused by microgravity may begin immediately after exposure to the microgravity environment, with the body gradually adapting around the second week. We speculate that the stability of the TLCPD in the mid-exposure period may be related to cerebrospinal fluid regeneration, gradually increasing the pressure difference and compensating for the gap between the bilateral pressures. Various subtypes of glial cells (such as microglial cells and astrocytes) are closely related to neurodegeneration under simulated microgravity. The early activation of microglial cells is positively correlated with the severity of subsequent optic nerve damage and can serve as a prognostic indicator of neurodegeneration<sup>[64-65]</sup> (Figure 9). In this study, the activation of neuroimmune cells was highly significant. In our previous research, we used minocycline (MINO) injection as an intervention to control neuroimmune activation. It is known that MINO can penetrate the BRB, inhibit pro-inflammatory microglial cells, and has been shown to prevent early axonal glial cell changes and improve the severity of neurodegeneration in ocular hypertension animal models<sup>[65-66]</sup>. Therefore, our research team also conducted interventions targeting neuroimmune activation and pressure changes. We continue to believe that changes in the dual-chamber ocular and brain pressure will be a crucial entry point for understanding simulated microgravity-induced damage. Furthermore, determining whether reversing this pressure pattern can serve as a method to protect against simulated microgravity conditions will be an important direction for future research.

Although this study provides valuable data on the effects of simulated microgravity on the retina and optic nerve,

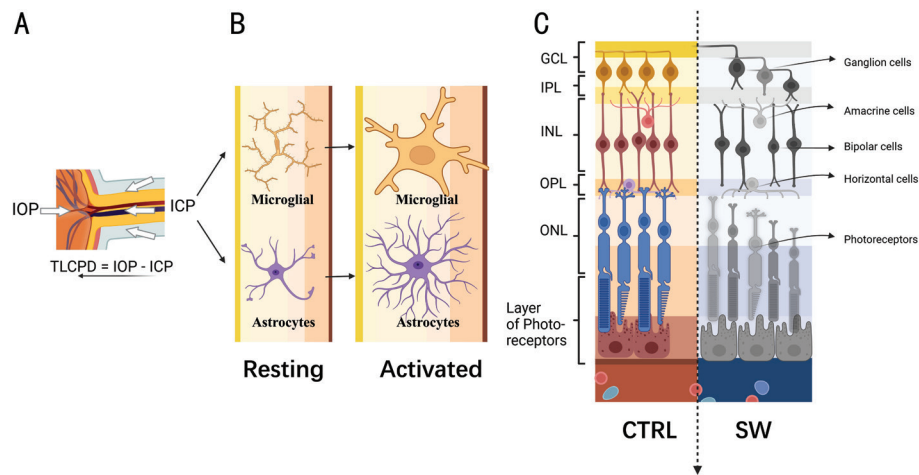


**Figure 9 Reversed TLCPD causes mechanical stress on the lamina cribrosa region of the retina, leading to damage of retinal nerve cells**

A: Under simulated microgravity, when ICP exceeds IOP, a pressure gradient directed anteriorly is generated. In this pathological state, the reversed pressure difference is considered in our study to cause damage to retinal photoreceptor cells, resulting in impaired visual function. B: Activation of two types of neuroimmune cells in our study—astrocytes and microglial cells—transitioning from a resting state to an activated state. C: Excessive activation of neuroimmune cells may ultimately damage retinal cells, as evidenced by findings in ERG, OMR, histopathological sections, and immunofluorescence staining. TLCPD: Trans-lamina cribrosa pressure difference; IOP: Intraocular pressure; ICP: Intracranial pressure; SW: Simulated microgravity; ERG: Electroretinography; OMR: Optomotor response; CTRL: Control.

some limitations remain. For instance, as mentioned earlier, ICP may be influenced by anesthetic conditions and body positioning, and the measurements only represent values during surgery, without reflecting ongoing changes. We did not perform genetic-level validation to explore which specific neuroimmune phenotypes were activated, which could have helped clarify the mechanisms through which neuroimmune activation leads to damage. Additionally, other research teams have identified the retinal pigment epithelium as a key site of damage in the overall microgravity-induced injury, a focus we did not explore. Neuroinflammation and oxidative stress may also contribute to the injury process. These areas will become ongoing research directions, and we will focus on identifying effective interventions for simulated microgravity.

#### ACKNOWLEDGEMENTS

**Conflicts of Interest:** Liu JS, None; Yan NQ, None; Mao YY, None; Xin C, None; Mou DP, None; Gao XX, None; Guo J, None; Wang NL, None; Zhu SQ, None.

#### REFERENCES

- 1 Mader TH, Gibson CR, Miller NR, *et al.* An overview of spaceflight-associated neuro-ocular syndrome (SANS). *Neurol India* 2019;67(Supplement):S206-S211.
- 2 Laurie SS, Vizzeri G, Taibbi G, *et al.* Effects of short-term mild hypercapnia during head-down tilt on intracranial pressure and ocular structures in healthy human subjects. *Physiol Rep* 2017;5(11):e13302.
- 3 Lee AG, Tarver WJ, Mader TH, *et al.* Neuro-ophthalmology of space flight. *J Neuroophthalmol* 2016;36(1):85-91.
- 4 Patel ZS, Brunstetter TJ, Tarver WJ, *et al.* Red risks for a journey to the red planet: The highest priority human health risks for a mission to Mars. *NPJ Microgravity* 2020;6(1):33.

- 5 Ong J, Tavakkoli A, Zaman N, *et al.* Terrestrial health applications of visual assessment technology and machine learning in spaceflight associated neuro-ocular syndrome. *NPJ Microgravity* 2022;8(1):37.
- 6 Zhang LF, Hargens AR. Spaceflight-induced intracranial hypertension and visual impairment: pathophysiology and countermeasures. *Physiol Rev* 2018;98(1):59-87.
- 7 Yiangou A, Mollan SP, Sinclair AJ. Idiopathic intracranial hypertension: a step change in understanding the disease mechanisms. *Nat Rev Neurol* 2023;19(12):769-785.
- 8 Zwart SR, Gibson CR, Gregory JF, *et al.* Astronaut ophthalmic syndrome. *FASEB J* 2017;31(9):3746-3756.
- 9 Willey JS, Britten RA, Blaber E, *et al.* The individual and combined effects of spaceflight radiation and microgravity on biologic systems and functional outcomes. *J Environ Sci Health C Toxicol Carcinog* 2021;39(2):129-179.
- 10 Norsk P. Adaptation of the cardiovascular system to weightlessness: surprises, paradoxes and implications for deep space missions. *Acta Physiol (Oxf)* 2020;228(3):e13434.
- 11 Dai XF, Ye SM, Chen XP, *et al.* Rodent retinal microcirculation and visual electrophysiology following simulated microgravity. *Exp Eye Res* 2020;194:108023.
- 12 Mao XW, Boerma M, Rodriguez D, *et al.* Combined effects of low-dose proton radiation and simulated microgravity on the mouse retina and the hematopoietic system. *Radiat Res* 2019;192(3):241-250.
- 13 Lee AG, Mader TH, Gibson CR, *et al.* Author correction: spaceflight associated neuro-ocular syndrome (SANS) and the neuro-ophthalmologic effects of microgravity: a review and an update. *NPJ Microgravity* 2020;6:23.
- 14 Rodríguez-Arzate CA, Noguez-Imm R, Reyes-Ortega P, *et al.* Potential contributions of the intrinsic retinal oscillations recording using non-

- invasive electroretinogram to bioelectronics. *Front Cell Neurosci* 2023;17:1224558.
- 15 Takita Y, Sugano E, Kitabayashi K, *et al.* Evaluation of local retinal function in light-damaged rats using multifocal electroretinograms and multifocal visual evoked potentials. *Int J Mol Sci* 2023;24(22):16433.
- 16 Prencipe M, Perossini T, Brancoli G, *et al.* The photopic negative response (PhNR): measurement approaches and utility in glaucoma. *Int Ophthalmol* 2020;40(12):3565-3576.
- 17 Wei DY, Mu YX, Xu XY, *et al.* Comparison of ocular changes after simulated long-term microgravity exposure between albino and non-albino rats. *Laboratory Animal Science* 2023;40(6):1-6.
- 18 Shen GF, Link SS, Tao XF, *et al.* Modeling a potential SANS countermeasure by experimental manipulation of the translaminal pressure difference in mice. *NPJ Microgravity* 2020;6:19.
- 19 Shen GF, Link S, Kumar S, *et al.* Characterization of retinal ganglion cell and optic nerve phenotypes caused by sustained intracranial pressure elevation in mice. *Sci Rep* 2018;8:2856.
- 20 Cheng Y, Lin DT, Wu S, *et al.* Cerebrospinal fluid pressure reduction induces glia-mediated retinal inflammation and leads to retinal ganglion cell injury in rats. *Mol Neurobiol* 2023;60(10):5770-5788.
- 21 Liu KC, Fleischman D, Lee AG, *et al.* Current concepts of cerebrospinal fluid dynamics and the translaminal cribrosa pressure gradient: a paradigm of optic disk disease. *Surv Ophthalmol* 2020;65(1):48-66.
- 22 Li XX, Zhang Z, Zeng HY, *et al.* Selective early glial reactivity in the visual pathway precedes axonal loss, following short-term cerebrospinal fluid pressure reduction. *Invest Ophthalmol Vis Sci* 2018;59(8):3394-3404.
- 23 Cheng Y, Wu S, Yan XJ, *et al.* Human Pro370Leu mutant myocilin induces the phenotype of open-angle glaucoma in transgenic mice. *Cell Mol Neurobiol* 2023;43(5):2021-2033.
- 24 Zhang LF, Chen JE, Ding ZP, *et al.* Cardiovascular deconditioning effects of long-term simulated weightlessness in rats. *Physiologist* 1993;36(1 Suppl):S26-S27.
- 25 Mao YY, Yang DY, Li J, *et al.* Finite element analysis of trans-lamina cribrosa pressure difference on optic nerve head biomechanics: the Beijing Intracranial and Intraocular Pressure Study. *Sci China Life Sci* 2020;63(12):1887-1894.
- 26 Srinivasan A, Srinivasan A, Ferland RJ. AutoSholl allows for automation of Sholl analysis independent of user tracing. *J Neurosci Methods* 2020;331:108529.
- 27 Young K, Morrison H. Quantifying microglia morphology from photomicrographs of immunohistochemistry prepared tissue using ImageJ. *J Vis Exp* 2018(136):57648.
- 28 Morey-Holton ER, Globus RK. Hindlimb unloading rodent model: technical aspects. *J Appl Physiol (1985)* 2002;92(4):1367-1377.
- 29 Mader TH, Gibson CR, Pass AF, *et al.* Optic disc edema, globe flattening, choroidal folds, and hyperopic shifts observed in astronauts after long-duration space flight. *Ophthalmology* 2011;118(10):2058-2069.
- 30 Frey MA, Mader TH, Bagian JP, *et al.* Cerebral blood velocity and other cardiovascular responses to 2 days of head-down tilt. *J Appl Physiol* 1993;74(1):319-325.
- 31 Payne SC, Bartlett CA, Harvey AR, *et al.* Myelin sheath decompaction, axon swelling, and functional loss during chronic secondary degeneration in rat optic nerve. *Invest Ophthalmol Vis Sci* 2012;53(10):6093-6101.
- 32 Lee AG, Mader TH, Gibson CR, *et al.* Space flight-associated neuro-ocular syndrome (SANS). *Eye (Lond)* 2018;32(7):1164-1167.
- 33 Kergoat H, Durand MJ. Correlating increased ocular and systemic blood pressures with neuroretinal function. *Aviat Space Environ Med* 1996;67(12):1174-1178.
- 34 Du ZJ, Yamamoto T, Ueda T, *et al.* Activated protein C rescues the retina from ischemia-induced cell death. *Invest Ophthalmol Vis Sci* 2011;52(2):987-993.
- 35 Van Ombergen A, Jillings S, Jeurissen B, *et al.* Brain tissue-volume changes in cosmonauts. *N Engl J Med* 2018, 379(17):1678-1680.
- 36 Roberts DR, Albrecht MH, Collins HR, *et al.* Effects of spaceflight on astronaut brain structure as indicated on MRI. *N Engl J Med* 2017;377(18):1746-1753.
- 37 Jasien JV, Samuels BC, Johnston JM, *et al.* Effect of body position on intraocular pressure (IOP), intracranial pressure (ICP), and translaminal pressure (TLP) via continuous wireless telemetry in nonhuman Primates (NHPs). *Invest Ophthalmol Vis Sci* 2020;61(12):18.
- 38 Pang RQ, Lin DT, Di XM, *et al.* Reference values for trans-lamina cribrosa pressure difference and its association with systemic biometric factors. *Eye (Lond)* 2023;37(11):2240-2245.
- 39 Sun D, Lye-Barthel M, Masland RH, *et al.* The morphology and spatial arrangement of astrocytes in the optic nerve head of the mouse. *J Comp Neurol* 2009;516(1):1-19.
- 40 May CA, Lütjen-Drecoll E. Morphology of the murine optic nerve. *Invest Ophthalmol Vis Sci* 2002;43(7):2206-2212.
- 41 Berdahl JP, Allingham RR. Intracranial pressure and glaucoma. *Curr Opin Ophthalmol* 2010;21(2):106-111.
- 42 Liang QF, Wang LY, Liu XY. Mechanism study of trans-lamina cribrosa pressure difference correlated to optic neuropathy in individuals with glaucoma. *Sci China Life Sci* 2020;63(1):148-151.
- 43 Zhang Z, Liu DL, Jonas JB, *et al.* Axonal transport in the rat optic nerve following short-term reduction in cerebrospinal fluid pressure or elevation in intraocular pressure. *Invest Ophthalmol Vis Sci* 2015;56(8):4257-4266.
- 44 Kato K, Sugawara A, Nagashima R, *et al.* Factors affecting photopic negative response recorded with RETeval system: study of young healthy subjects. *Transl Vis Sci Technol* 2020;9(9):19.
- 45 Zhang Z, Wu S, Jonas JB, *et al.* Dynein, kinesin and morphological changes in optic nerve axons in a rat model with cerebrospinal fluid pressure reduction: the Beijing Intracranial and Intraocular Pressure (iCOP) study. *Acta Ophthalmol* 2016;94(3):266-275.
- 46 Zhao HW, Zhao J, Hu LN, *et al.* Effect of long-term weightlessness on retina and optic nerve in tail-suspension rats. *Int J Ophthalmol* 2016;9(6):825-830.

- 47 Fan W, Huang WD, Chen JY, *et al.* Retinal microglia: functions and diseases. *Immunology* 2022;166(3):268-286.
- 48 Karlstetter M, Scholz R, Rutar M, *et al.* Retinal microglia: just bystander or target for therapy *Prog Retin Eye Res* 2015;45:30-57.
- 49 Imai Y, Ibata I, Ito D, *et al.* A novel gene *iba1* in the major histocompatibility complex class III region encoding an EF hand protein expressed in a monocytic lineage. *Biochem Biophys Res Commun* 1996;224(3):855-862.
- 50 Guo L, Choi S, Bikkannavar P, *et al.* Microglia: key players in retinal ageing and neurodegeneration. *Front Cell Neurosci* 2022;16:804782.
- 51 Arroba AI, Valverde ÁM. Modulation of microglia in the retina: new insights into diabetic retinopathy. *Acta Diabetol* 2017;54(6):527-533.
- 52 Habib P, Slowik A, Zendedel A, *et al.* Regulation of hypoxia-induced inflammatory responses and M1-M2 phenotype switch of primary rat microglia by sex steroids. *J Mol Neurosci* 2014;52(2):277-285.
- 53 Mao XW, Byrum S, Nishiyama NC, *et al.* Impact of spaceflight and artificial gravity on the mouse retina: biochemical and proteomic analysis. *Int J Mol Sci* 2018;19(9):2546.
- 54 Li SQ, Song QY, Wu B, *et al.* Structural damage to the rat eye following long-term simulated weightlessness. *Exp Eye Res* 2022;223:109200.
- 55 Dai XF, Bao JH, Chen XP, *et al.* Effect of simulated microgravity on the photopic negative response of flash electroretinogram in adult mice. *Chinese Journal of Ocular Fundus Diseases* 2019;35(4):379-384.
- 56 Liao F, Liu HT, Milla-Navarro S, *et al.* Origin of retinal oscillatory potentials in the mouse, a tool to specifically locate retinal damage. *Int J Mol Sci* 2023;24(4):3126.
- 57 Dai XF, Bao JH, Chen XP, *et al.* Impact of simulated microgravity on flash electroretinogram and retinal microcirculation in adult mice. *Guoji Yanke Zazhi (Int Eye Sci)* 2020;20(1):27-31.
- 58 Salerni F, Repetto R, Harris A, *et al.* Biofluid modeling of the coupled eye-brain system and insights into simulated microgravity conditions. *PLoS One* 2019;14(8):e0216012.
- 59 Overbey EG, da Silveira WA, Stanboully S, *et al.* Spaceflight influences gene expression, photoreceptor integrity, and oxidative stress-related damage in the murine retina. *Sci Rep* 2019;9(1):13304.
- 60 Tombran-Tink J, Barnstable CJ. Space flight environment induces degeneration in the retina of rat neonates. *Adv Exp Med Biol* 2006;572:417-424.
- 61 Nday CM, Frantzidis C, Jackson G, *et al.* Neurophysiological changes in simulated microgravity: an animal model. *Neurol India* 2019;67(Supplement):S221-S226.
- 62 Laurie SS, Lee SMC, Macias BR, *et al.* Optic disc edema and choroidal engorgement in astronauts during spaceflight and individuals exposed to bed rest. *JAMA Ophthalmol* 2020;138(2):165-172.
- 63 Mu YX, Wei DY, Yao L, *et al.* Choroidal circulation disturbance is an initial factor in outer retinal degeneration in rats under simulated weightlessness. *Front Physiol* 2023;14:1198862.
- 64 Hu X, Zhao GL, Xu MX, *et al.* Interplay between Müller cells and microglia aggravates retinal inflammatory response in experimental glaucoma. *J Neuroinflammation* 2021;18(1):303.
- 65 Bosco A, Romero CO, Breen KT, *et al.* Neurodegeneration severity can be predicted from early microglia alterations monitored *in vivo* in a mouse model of chronic glaucoma. *Dis Model Mech* 2015;8(5):443-455.
- 66 Bordone MP, González Fleitas MF, Pasquini LA, *et al.* Involvement of microglia in early axoglial alterations of the optic nerve induced by experimental glaucoma. *J Neurochem* 2017;142(2):323-337.